Korean J. Chem. Eng., 37(7), 1226-1232 (2020)
DOI: 10.1007/s11814-020-0520-7

pISSN: 0256-1115
eISSN: 1975-7220

Silver-doped ZnO for photocatalytic degradation of methylene blue

Dayoung Kwon and Jongsung Kim†

Department of Chemical and Biological Engineering, Gachon University,
Seongnam-daero 1342, Seongnam-si, Gyeonggi-do 13120, Korea
(*Received 2 October 2019 • Revised 20 February 2020 • Accepted 27 February 2020*)

Abstract−Removal of organic dyes from wastewater has become an important issue because of their carcinogenic and mutagenic effects. In this study, we prepared Ag-doped ZnO (Ag_ZnO) photocatalysts containing various amounts of Ag (0.05-0.5 mol%) by a hydrothermal process followed by calcination at 500 °C and evaluated the photocatalytic degradation of methylene blue (MB) under sunlight irradiation. The incorporation of Ag into the ZnO lattice and the hexagonal wurtzite structure of the prepared catalysts could be confirmed by X-ray photoelectron spectroscopy and powder X-ray diffraction analysis. BET analysis shows that the pore volume and pore size was increased with doping Ag into ZnO. The photocatalytic degradation of methylene blue followed a pseudo-first-order kinetics and the rate constant for dye degradation with 0.1% mol Ag was almost three-times bigger than that with bare ZnO. Our study shows that the photocatalytic activity of ZnO toward MB degradation under sunlight can be effectively enhanced by doping with Ag.

Keywords: Silver-doped ZnO, Hexagonal Structure, Sunlight, Photocatalyst, Methylene Blue

INTRODUCTION

Water pollution due to uncontrolled release of industrial toxic organic dyes has become a major cause of environmental pollution. Dyes are considered industrial organic pollutants because they are very toxic, carcinogenic, and mutagenic [1]. Photodegradation of dyes with suitable active catalysts has economical merits because abundant natural solar energy can be used in such processes. Various semiconductors have been used for the photocatalytic degradation of environmentally hazardous organic dyes [2]. Semiconductor-based photocatalysis is a green and feasible technology that uses direct conversion of solar energy into chemical energy, thus driving many kinds of chemical transformations. This technology has attracted considerable attention in recent years in the remediation of environmental pollution [3]. Metal oxide photocatalysts, such as zinc oxide (ZnO), titanium dioxide (TiO_2), iron oxide (Fe_2O_3), and zirconium oxide (ZrO_2), have been used extensively in the degradation of organic pollutants in water and air because of their ability to generate charge carriers stimulated by solar energy [4,5]. ZnO is a representative n-type semiconductor with a wide band gap of 3.37 eV that shows photocatalytic activity under UV light [6]. It has many great optical and electrical properties that can be used as photochemical sensors and catalysts. Among various metal-oxide photocatalysts, ZnO has shown excellent chemical and photochemical stability, non-toxicity, low production cost, and a large exciton binding energy [7]. However, its major drawback is that it is susceptible to deterioration upon exposure to UV irradiation in aqueous solutions, a phenomenon usually referred to as photocorrosion [8]. Doping of transition metal into ZnO can increase the photocatalytic activity by introducing charge traps for the photogenerated carrier and suppressing charge carrier recombination [9]. Ag is a stable, non-toxic metal that has the highest electrical conductivity of all metals [10]. There have been several reports on the synthesis of nanosized metal oxides via a variety of synthetic routes such as hydrothermal, microwave, and sol-gel syntheses. Among them, the hydrothermal method is widely used because of the low cost, low operational temperature, and high yield involved and the control over the shape and dimension of nanomaterials it offers when the reaction time, temperature, and capping agent are tuned [11]. Herein, we report the preparation of Ag doped ZnO by a hydrothermal process and the photocatalytic decomposition behavior of methylene blue under irradiation by sunlight. A dye degradation ratio (C/Co) of 92.9% was achieved by 0.1% Ag_ZnO.

EXPERIMENTAL

1. Preparation of Ag_ZnO

All chemicals were of analytical grade and used as received without further purification. Typically, a 0.15 M zinc nitrate hexahydrate ($Zn(NO_3)_2{\cdot}6H_2O$) solution was prepared in 40 mL of ethanol. Afterwards, silver nitrate ($AgNO_3$) was added to prepare 0.1, 0.2, 0.3, 0.4 and 0.5 mol% silver doped ZnO. The solution was stirred vigorously for 30 min, and a 1 M sodium hydroxide (NaOH) ethanol solution was added dropwise to the above mixture to maintain the pH at 11. After complete dissolution, the solution was sealed in a 100 mL Teflon-lined autoclave reactor and heated for 3 h at a constant temperature of 200 °C. Then, the autoclave reactor was cooled to room temperature and the reacted solution was centrifuged at 8,500 rpm for 10 min. The precipitate was collected, washed with distilled water and ethanol several times to remove any impurities, and dried overnight at 70 °C. Finally, the Ag_ZnO product was calcined at 500 °C for 2 h using a ramping rate of 10 °C/min.

2. Photocatalytic Measurements

The photocatalytic efficiencies of the ZnO and Ag_ZnO photo-

†To whom correspondence should be addressed.
E-mail: jongkim@gachon.ac.kr
Copyright by The Korean Institute of Chemical Engineers.

catalyst samples were evaluated by measuring the optical absorbance of a methylene blue solution with the prepared photocatalysts under sunlight irradiation. A 100 W halogen lamp (JB-420, Nantong Haisheng Optical Co., Ltd., Shanghai, China) was used as the sunlight irradiation source to activate the photocatalytic reaction. Typically, 50 mg of the prepared photocatalyst was dispersed in 100 mL of a 10-ppm methylene blue dye solution in a 500 mL glass beaker. To maintain the adsorption-desorption equilibrium, the mixture was continuously stirred for 30 min in the dark without light irradiation, and then light was switched on. Every 30 min, 3 mL of the sample solution was pipetted out and centrifuged to discard the photocatalyst. Finally, the extent of photodegradation was analyzed by measuring the decrease in the absorbance intensity of methylene blue using a UV-vis spectrophotometer.

3. COD Measurements

COD was measured by open reflux method: 20 ml of dye solution was mixed with sulfuric acid, silver sulfate, and 0.005 M potassium permanganate solution in a round bottom flask. The reaction mixture was refluxed for 30 min and allowed to cool naturally at room temperature. Then, 0.0125 M sodium oxalates solution was added into the mixture. Finally, COD was measured by titration of 0.005 M of potassium permanganate solution.

4. Characterization

The morphology of the Ag_ZnO samples was studied by field-emission scanning electron microscopy (FE-SEM, S-4700, Hitachi) at Smart Materials Research Center for IoT (SMRCI) in Gachon University. The crystal structure of the samples was studied by powder X-ray diffraction (XRD) with an Ultima IV diffractometer using Cu Kα as the X-ray source; the 2-theta range was set at 2-90°. The surface electronic states of the photocatalysts were analyzed by X-ray photoelectron spectroscopy (XPS, Multilab-2000) with a twin anode (Al Kα, hν=1,486.6 eV). The absorbance spectra were recorded using a UV-vis spectrophotometer (Varian Cary 100). The specific surface area was determined from the nitrogen adsorption/desorption isotherms using the BET (Brunauer-Emmett-Teller) method (3 Flex Physisorption).

RESULTS AND DISCUSSION

1. Crystal Structure and Morphology of Ag_ZnO Photocatalysts

Powder XRD analysis was performed to identify the crystal structure, lattice parameter, and crystallite size of the pure ZnO and

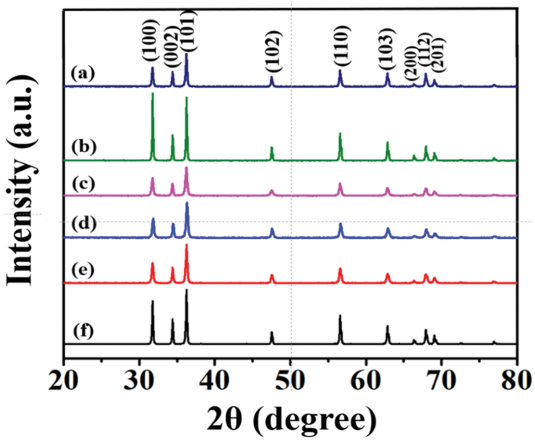


Fig. 1. XRD patterns of (a) bare ZnO, (b) 0.1% Ag_ZnO, (c) 0.2% Ag_ZnO, (d) 0.3% Ag_ZnO, (e) 0.4% Ag_ZnO, and (f) 0.5% Ag_ZnO photocatalyst.

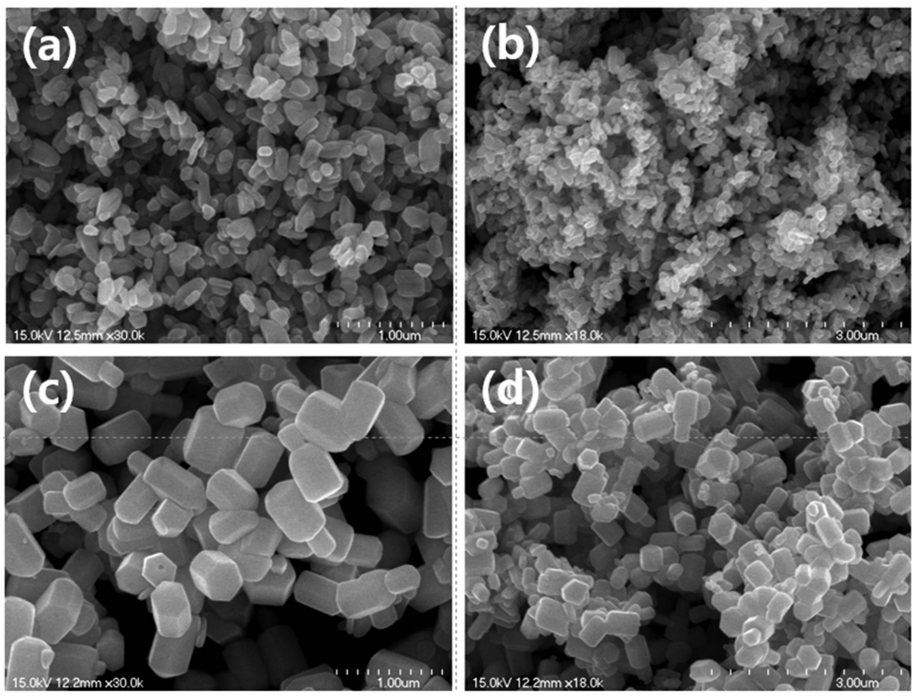


Fig. 2. FE-SEM images of (a), (b) bare ZnO and (c), (d) 0.1% Ag_ZnO photocatalyst.

Ag_ZnO nanoparticles. The X-ray diffraction patterns of ZnO, and Ag_ZnO photocatalysts are shown in Fig. 1. The peaks obtained for ZnO and Ag_ZnO photocatalyst at 2θ=31.8, 34.4, 36.3, 47.5, 56.6, 62.9, 66.3, 67.9, and 69.0 matched with the lattice planes (100), (002), (101), (102), (110), (103), (200), (112), and (201), respectively [12,13]. The lattice plane (101) demonstrated anisotropic nature and suggested the direction of crystallinity [14]. Thus, the XRD results confirmed that the samples could exhibit a hexagonal wurtzite structure, which was in good agreement with JCPDS card no 36-1451 [15]. Among the samples, 0.1% Ag_ZnO showed XRD peaks with strong intensity. This implies a strong hexagonal wurtzite structure. The XRD pattern also shows that, on doping with Ag into ZnO, the hexagonal wurtzite structure of ZnO did not change.

The surface morphology of ZnO and Ag_ZnO photocatalysts was studied by FE-SEM. Fig. 2 shows the SEM images of ZnO and 0.1% Ag_ZnO photocatalysts. Fig. 2(a) and (b) show that ZnO powders were either spherical or short and rod-shaped [16]. 1% Ag_ZnO (Fig. 2(c), (d)) showed particles a little larger than bare ZnO but had a hexagonal structure with a [0001] facet [17]. This coincided with the XRD results, which showed that 0.1% Ag_ZnO exhibited strong XRD peaks. The morphology of bare ZnO and Ag_ZnO photocatalysts was different but both exhibited a short rod-shaped structure. 0.1% Ag doped ZnO shows decrease in agglomeration compared to bare ZnO, which leads to more regular shape [18]. There is a possible mechanism of change in shape by doping Ag into ZnO, where Ag^+ affected the growth tendency of ZnO. When Ag^+ ions are added to the reaction solution, Ag^+ and OH^- will first interact to generate AgOH precipitation which consumes a part of the alkaline ions in the solution, then the ZnO tends to grow in hexagonal structure. [19]. This decrease in agglomeration and regular organization of ZnO by Ag doping can improve the photocatalytic activity. According to the SEM micrographs, it was evident that the morphology of ZnO changed to a clear hexagonal shape on doping with Ag [20].

2. BET Surface Area Analysis

The surface area of bare ZnO and 0.1%Ag_ZnO was determined using BET analysis. Larger surface area of the photocatalyst can have enhanced photocatalytic activity because it can provide more active site to adsorb pollutants [21]. Fig. 3 shows surface areas of ZnO and 0.1%Ag_ZnO photocatalysts which were determined by N_2 adsorption-desorption isotherm. The BET surface area of ZnO and 1%Ag_ZnO is 6.3141 m^2/g and 7.4929 m^2/g, respectively. BET surface of 0.1%Ag_ZnO is higher than the bare ZnO. Table 1 shows the BET surface area, total pore volume and pore size. Total pore volume and pore size of ZnO are 0.0160 cm^2/g and 101.2736 Å, whereas those of 0.1%Ag_ZnO are 0.0212 cm^2/g and 113.1293 Å, respectively. The BET analysis shows that total pore

Table 1. Surface properties of ZnO and 0.1%Ag_ZnO

Properties	ZnO	0.1%Ag_ZnO
BET surface area	6.3143 m^2/g	7.4929 m^2/g
Total pore volume	0.0160 cm^3/g	0.0212 cm^3/g
Pore size	101.2736 Å	113.1293 Å

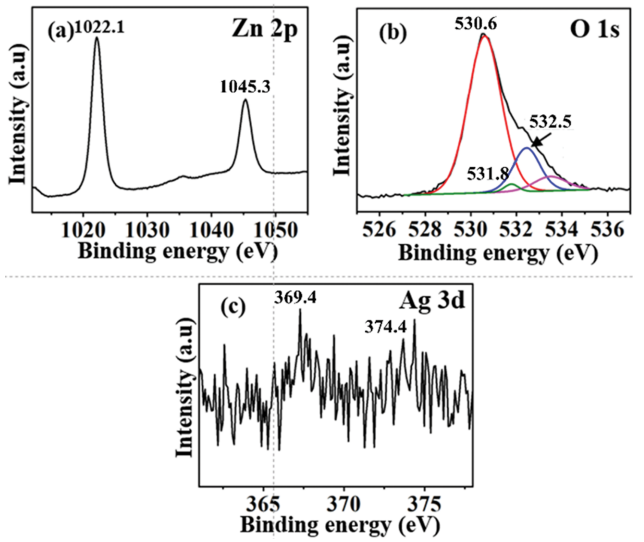


Fig. 4. High-resolution XPS profiles of (a) Zn 2p, (b) O 1s, and (c) Ag 3d for 0.1% Ag_ZnO photocatalyst.

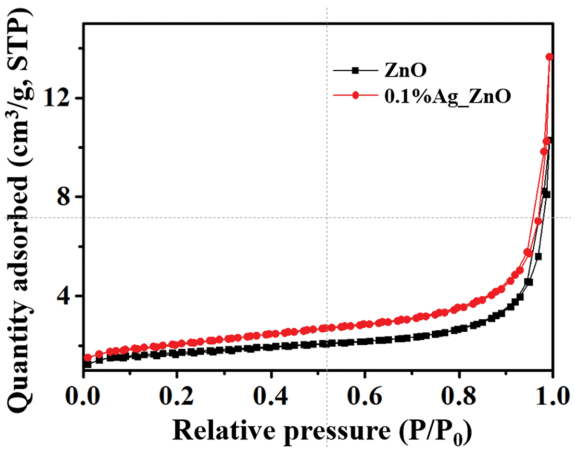


Fig. 3. N_2 adsorption-desorption isotherms of ZnO and 0.1%Ag_ZnO.

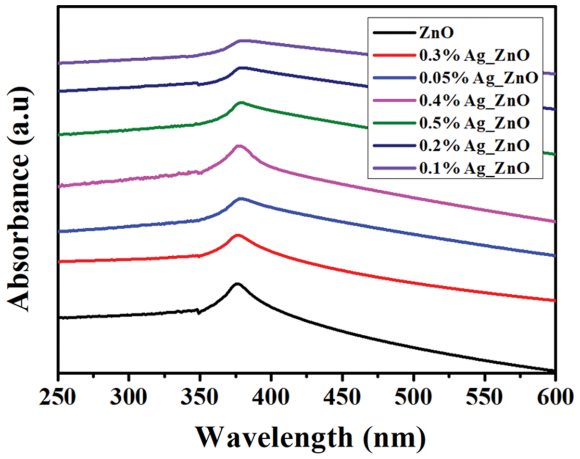


Fig. 5. UV-vis absorption spectra of ZnO and Ag_ZnO photocatalysts with various Ag concentrations.

volume and pore size of ZnO were increased by doping with Ag, which in turn increased the surface active sites of catalysts [22].

3. Chemical State of Ag_ZnO Photocatalysts

XPS was conducted to analyze the distribution and oxidation state of the constituent elements in Ag_ZnO. Fig. 3 shows the high-resolution XPS spectra of Zn 2p, O 1s, and Ag 3d. As seen in Fig. 4(a), Zn 2p of Ag_ZnO shows two peaks at 1,022.1 and 1,045.3 eV, which could be ascribed to Zn 2p3/2 and Zn 2p1/2, respectively [23]. In Fig. 4(b), the O 1s peak position at the binding energy of 530.6 eV could be assigned to O^{2-} ions involved in Zn-O bonds of the wurtzite structure of ZnO [24]. A peak at 531.8 eV sufficiently indicates Ag-O bond formation in Ag_ZnO [25]. It was noted that Ag was doped into ZnO, which contributed to enhancing the photocatalytic activity. A peak at 532.5 eV could be attributed to oxygen

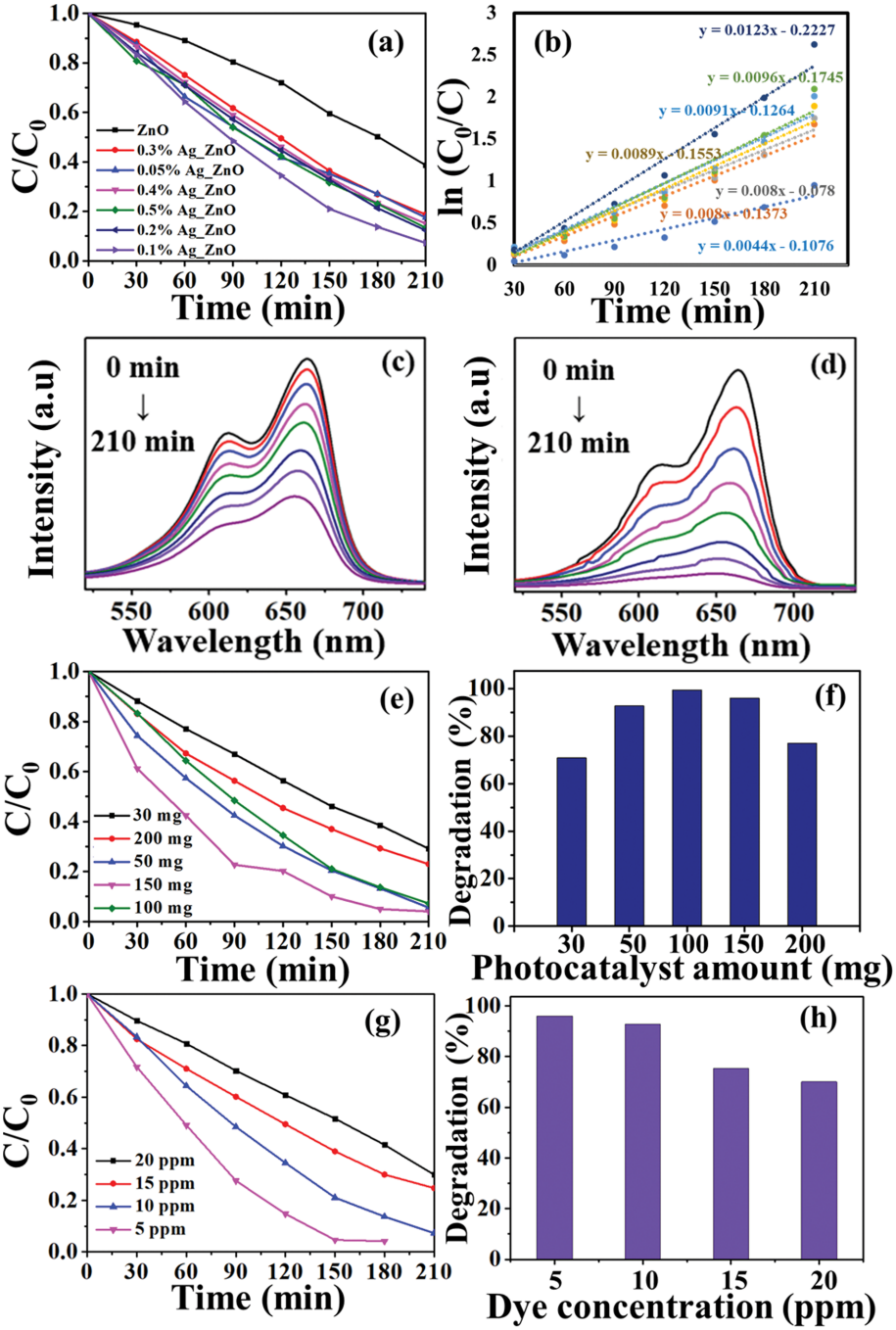


Fig. 6. (a) C/C_0 vs time plot showing degradation of methylene blue (MB) dye in the presence of bare ZnO and Ag_ZnO photocatalyst under sunlight irradiation up to 210 min; (b) kinetic plot of photocatalytic degradation of MB; (c), (d) gradual decrease in the absorption of MB with time in the presence of ZnO and 0.1% Ag_ZnO photocatalyst, respectively; (e), (f) C/C_0 vs time plot showing degradation of MB and final degradation % of MB with various amounts of 0.1% Ag_ZnO; (g), (h) degradation with time and final degradation % of various concentrations of MB with 0.1% Ag_ZnO.

on the surface hydroxyl group [26]. In Fig. 4(c), two peaks can be seen at 369.4 and 374.4 eV, which can be attributed to Ag 3d5/2 and Ag 3d3/4, respectively [27]. Furthermore, these two peaks indicate the presence of AgO and Ag_2O along with metallic silver [28]. The incorporation of metallic Ag into the ZnO crystal lattice was thus confirmed by high-resolution XPS analysis.

4. Optical Bandgap Study

Fig. 5 shows UV-vis absorption spectra of ZnO and Ag_ZnO photocatalysts UV-vis absorption spectrum represents the available change in the energy gap [29]. The optical bandgap (Eg) can be obtained from λ_{max} by Eg=1240/λ_{max} [30]. The peaks of bare ZnO and 0.3, 0.05, 0.4, 0.5, 0.2 and 0.1% doped ZnO were observed at 376, 377, 377, 377, 379, 379 and 381 nm, which correspond to optical bandgap of 3.30, 3.29, 3.29, 3.29, 3.27, 3.27 and 3.25 eV, respectively. The absorption peak at 376 nm of bare ZnO indicates wurtzite crystal structure [31]. As the Ag dopant concentration is increased, the absorption peak is red shifted, which coincides with the previous report [32]. The decrease in the optical band gap with dopant concentration is due to enhancement in the carrier species in valence band and conduction band [33].

5. COD Measurement

The chemical oxygen demand can estimate the organic strength of methylene blue dye in terms of total quantity of oxygen required for the oxidation of organic matter to CO_2 and water [34]. It has been observed that the COD of the methylene blue solution decreases from 28 mg/L to 4 mg/L after photodegradation, indicating that about 85% of dye is completely degraded. The large reduction in COD clearly is consistent with the photodegradation results measured by UV absorption [35].

6. Photocatalytic Degradation of Methylene Blue under Sunlight

Fig. 6(a) shows the photocatalytic performance of undoped ZnO and Ag_ZnO photocatalysts toward the degradation of methylene blue under sunlight irradiation. It shows the variation in C/C_0 (where C_0 is the initial concentration and C is the present concentration) of methylene blue with respect to time in the presence of various amounts of photocatalysts. As observed, at 210 min, the amount of dye degradation was the highest for the samples with the 0.1% Ag_ZnO photocatalyst. The final dye degradation percentage with bare ZnO, 0.3%, 0.05%, 0.4%, 0.5%, 0.2% and 0.1% Ag_ZnO was 61.8, 81.5, 82.6, 85.2, 86.8, 87.9, and 92.9% respectively. Kinetic studies were performed to evaluate the dye degradation rate employing the Langmuir-Hinshelwood kinetics model. Fig. 6(b) shows the plot of ln C_0/C vs time [36]. The photocatalytic degradation of methylene blue followed a pseudo-first-order kinetics, which could be modeled by the following equation

$$\ln\frac{C_0}{C} = kt \quad (1)$$

where k (min^{-1}) is the pseudo-first-order rate constant [37]. The rate constant was calculated to be 0.0123, 0.0096, 0.0971, 0.089, 0.080, 0.080 and 0.0044 min^{-1} with 0.1, 0.2, 0.5, 0.4, 0.05, 0.3% Ag_ZnO, and bare ZnO, respectively. More importantly, the rate constant for dye degradation with 0.1% mol Ag was almost three-times bigger than that with bare ZnO. Fig. 6(c) and (d) show the gradual decrease in the methylene blue absorption peak intensity in the presence of ZnO and 0.1% Ag_ZnO, respectively. The figures show significant degradation of methylene blue for the 0.1% Ag_ZnO photocatalyst compared with that obtained using pure ZnO. This means that the photocatalytic efficiency was significantly enhanced by doping Ag into the ZnO lattice. Fig. 6(e) shows plot of C/C_0 vs time for different amount of catalyst and (f) shows plot of degradation efficiency vs photocatalyst amount for the degradation of methylene blue dye with 0.1% Ag_ZnO. The final dye degradation percentage with 30, 50, 100, 150 and 200 mg of 0.1% Ag_ZnO was 70.9, 92.9, 94.4, 96.0, and 70.9%, respectively. With the increasing photocatalyst amount, the degradation efficiency was increased and 150 mg catalyst shows highest degradation efficiency. However, above 150 mg, the degradation efficiency was decreased, which may be due to the scattering of light. Fig. 6(g) shows plots of C/C_0 vs time for different concentration of dye and (h) shows a plot of degradation efficiency vs photocatalyst amount for the degradation of methylene blue dye with 0.1% Ag_ZnO. The final degradation percentage of dye of 5, 10, 15 and 20 ppm was 95.9, 92.7, 75.3 and 70.1, respectively. With increasing dye concentration, degradation efficiency was decreased and dye of 5 ppm shows highest efficiency.

Fig. 7 shows the mechanism of the charge transfer process occurring in the Ag_ZnO photocatalyst during photodegradation of methylene blue under sunlight illumination. In the presence of oxygen defects or metal nanoparticles on ZnO surface, the separation of photo generated electron-hole pair is enhanced. Ag promoted the charge transfer of photogenerated charge carriers [38]. When the Ag_ZnO was exposed to solar irradiation, the sunlight excited the electrons of the photocatalyst to the conduction band leaving the valence band to form holes through surface plasmon resonance [39]. Then the plasmon-induced electrons of silver dopants were quickly injected into the ZnO conduction band, then ZnO trapped electrons and Ag trapped holes reacted with the pre-adsorbed oxygen and hydroxyl group (-OH) [40]. Photoelectrons were adsorbed to O_2 and turned oxygen to a superoxide anion ($O^{\cdot -2}$). And the photogenerated holes turned water molecule to strong hydroxyl radicals (·OH) [41]. These superoxide anion ($O^{\cdot -2}$) and hydroxyl radicals (·OH) can degrade methylene blue to smaller

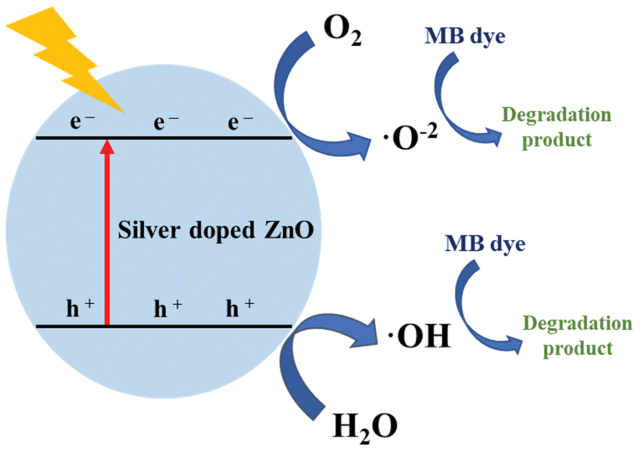


Fig. 7. Schematic illustration of photocatalytic charge transfer process in Ag_ZnO photocatalyst.

Table 2. Comparison of the photocatalytic performance of Ag_ZnO in photodegradation of dyes

Synthesis method	Dye	Degradation time	Degradation efficiency (%)	Ref.
Chemical co-precipitation	Methyl orange, methylene blue, and 4-nitrophenol	4 hours	85	[42]
Chemical precipitation	Methylene Blue	300 min	95	[43]
Laser-induction	Methylene Blue	8 hours	90	[44]
Spray coating	Methyl orange	7 hours	60	[45]
Sol-gel	Methylene blue	5 hours	67	[46]
Hydrothermal microwave heating synthesis	Methylene blue	5 hours	40	[47]
Polymer-assisted freeze-drying method	Methylene blue	5 hours	90	[48]
Wet synthesis method	Phenol	240 min	50	[49]
Hydrothermal	Methylene blue	210 min	92	This Work

species. In degradation product, ·OH radical can break various bonds in the dye (C-N, C=N, C-S, N=N, C-C etc), which leads to the conversion of dye into CO_2 and inorganic ions (NH_4^+, NO_3^- etc) [38]. With this process, Ag_ZnO provided better photocatalytic effects for the degradation of methylene blue compared to bare ZnO.

Table 2 shows the comparison of photocatalytic dye degradation with Ag_ZnO previously reported and the present work. Various methods were used for the preparation of Ag_ZnO including chemical precipitation, laser induction, spray coating, sol-gel, hydrothermal microwave heating synthesis, polymer-assisted freeze-drying method, wet synthesis method and hydrothermal process. Among them, the present work shows the shortest degradation time for dye degradation over 90%.

CONCLUSION

Silver-doped ZnO photocatalysts were prepared by a low-temperature hydrothermal process followed by calcination. Ag doping into ZnO can enhance the photocatalytic degradation of methylene blue under sunlight irradiation. The doping of Ag into the ZnO lattice was confirmed by XPS. The SEM images showed that the as-prepared Ag_ZnO had a hexagonal structure. The dye degradation percentage with bare ZnO and 0.3, 0.05, 0.4, 0.5, 0.2, and 0.1% Ag_ZnO photocatalyst was 61.8, 81.5, 82.6, 85.2, 86.8, 87.9, and 92.9, respectively. The photocatalytic degradation of methylene blue followed pseudo-first-order kinetics. The rate constant for dye degradation with 0.1 mol% Ag was almost three-times bigger than that with ZnO. Thus, doping Ag into ZnO provided better photocatalytic activity for the degradation of methylene blue compared to that of bare ZnO.

ACKNOWLEDGEMENTS

We thank the SMRCI at Gachon University for the instrumental support (SEM). This work was financially supported by the GRRC program (2018-A01) of Gachon University and the Human Resources Development of Korea Institute of Energy Technology Evaluation and Planning (KETEP) grant funded by the Korea government Ministry of Knowledge Economy (No. 20194030202440).

REFERENCES

1. U. Alam, A. Khan, D. Ali, D. Bahnemann and M. Muneer, *RSC Adv.*, **8**, 17582 (2018).
2. C. A. Jaramillo-Páez, J. A. Navío, M. C. Hidalgo and M. Macías, *Catal. Today*, **313**, 12 (2018).
3. C. Li, Y. Xu, W. Tu, G. Chen and R. Xu, *Green Chem.*, **19**, 882 (2017).
4. N. M. Flores, U. Pal, R. Galeazzi and A. Sandoval, *RSC Adv.*, **4**, 41099 (2014).
5. M. M. Khan, S. F. Adil and A. Al-Mayouf, *J. Saudi Chem. Soc.*, **19**, 462 (2015).
6. R. M. Kakhki, R. Tayebee and F. Ahsani, *J. Mater. Sci.: Mater. Electron.*, **28**, 5941 (2017).
7. A. Phuruangrat, P. Dumrongrojthanath, N. Ekthammathat, S. Thongtem and T. Thongtem, *J. Nanomater.*, **2014**, 59 (2014).
8. M. F. Khan, A. H. Ansari, M. Hameedullah, E. Ahmad, F. M. Husain, Q. Zia, U. Baig, M. R. Zaheer, M. M. Alam, A. M. Khan, Z. A. AlOthman, I. Ahmad, G. M. Ashraf and Z. A. AlOthman, *Sci. Rep.*, **6**, 27689 (2016).
9. N. F. Hamedani and F. Farzaneh, *J. Sci. I. R. Iran*, **17**, 231 (2006).
10. P. Govindhan and C. Pragathiswaran, *Natl. Acad Sci. Lett.*, **42**, 323 (2019).
11. R. Bomila, S. Srinivasan, S. Gunasekaran and A. Manikandan, *J. Supercond Nov. Magn.*, **31**, 855 (2018).
12. A. Riaz, A. Ashraf, H. Taimoor, S. Javed, M. A. Akram, M. Islam, M. Mujahid, L. Ahmad and K. Saeed, *Coatings*, **9**, 202 (2019).
13. S. Agnihotri, G. Bajaj, S. Mukherji and S. Mukherji, *Nanoscale*, **7**, 7415 (2015).
14. Y. J. Jose, M. Manjunathan and S. J. Selvaraj, *J. Nanostructure Chem.*, **7**, 259 (2017).
15. R. Bomila, S. Srinivasan, S. Gunasekaran and A. Manikandan, *J. Supercond Nov. Mahn.*, **31**, 855 (2018).
16. X. Chen, Z. Wu, D. Liu and Z. Gao, *Nanoscale Res. Lett.*, **12**, 143 (2017).
17. M. S. Azmina, R. M. Nor, H. A. Rafaie, N. S. A. Razak, S. F. A. Sani and Z. Osman, *Appl. Nanosci.*, **7**, 885 (2017).
18. R. Singh, P. B. Barman and D. Sharma, *J. Mater. Sci.: Mater.*, **28**, 5705 (2017).
19. X. Yu, Z. Li, K. Dang, Z. Zhang, L. Gao, L. Duan, Z. Jiang, J. Fan

and P. Zhao, *J. Mater. Sci.: Mater.*, **29**, 8729 (2018).
20. M. R. Islam, M. Rahman, S. F. U Farhad and J. Podder, *SURF INTER.*, **16**, 120 (2019).
21. A. Senthilraja, B. Krishnakumar, B. Subash, A. J. Sobral, M. Swaminathan and M. Shanthi, *J. Ind. Eng. Chem.*, **33**, 51 (2016).
22. R. Singh, P. B. Barman and D. Sharma, *J. Mater. Sci.: Mater.*, **28**, 5705 (2017).
23. R. Al-Gaashani, S. Radiman, A. R. Daud, N. Tabet and Y. Al-Douri, *Ceram. Int.*, **39**, 2283 (2013).
24. W. Bai, Z. Zhang, W. Tian, X. He, Y. Ma, Y. Zhao and Z. Chai, *J. Nanoparticle Res.*, **12**, 1645 (2010).
25. Y. Liu, H. Liu, Q. Zhang and T. Li, *RSC Adv.*, **7**, 3515 (2017).
26. M. E Ashebir, G. M. Tesfamariam, G. Y. Nigussie and T. W. Gebreab, *J. Nanomater.*, **2018**, 9 (2018).
27. M. Navaneethan, G. K. Mani, S. Ponnusamy, K. Tsuchiya, C. Muthamizhchelvan, S. Kawasaki and Y. Hayakawa, *J. Alloys Compd.*, **698**, 555 (2017).
28. S. Ghosh, V. S. Goudar, K. G. Padmalekha, S. V. Bhat, S. S. Indi and H. N. Vasan, *RSC Adv.*, **2**, 930 (2012).
29. B. Pal and P. K. Giri, *Int. J. Appl.*, **108**, 084322 (2010).
30. A. N. Kadam, T. G. Kim, D. S. Shin, K. M. Garadkar and J. Park, *J. Alloys Compd.*, **710**, 102 (2017).
31. R. Wahab, S. G. Ansari, Y. S. Kim, H. K. Seo, G. S. Kim, G. Khang and H. S. Shin, *Mater. Res.*, **42**, 1640 (2007).
32. S. M. Hosseini, I. A. Sarsari, P. Kameli and H. Salamati, *J. Alloys Compd.*, **640**, 408 (2015).
33. R. Singh, K. Verma, T. Singh, P. B. Barman and D. Sharma, *Mater. Res. Express.*, **5**, 025035 (2018).
34. M. A. Ahmed, M. A. Messih, E. F. El-Sherbeny, S. F. El-Hafez and A. M. Khalifa, *J. Photochem. Photobiol.*, **346**, 77 (2017).
35. S. Chowdhury and K. G. Bhattacharyya, *SN Appl. Sci.*, **1**, 87 (2019).
36. S. Agnihotri, S. Mukherji and S. Mukherji, *Nanoscale*, **5**, 7328 (2013).
37. J. Feng, D. Fan, Q. Wang, L. Ma, W. Wei, J. Xie and J. Zhu, *Colloid Surf. A Physicochem. Eng. Aap.*, **520**, 743 (2017).
38. X. Yu, Z. Li, K. Dang, Z. Zhang, L. Gao, L. Duan, Z. Jiang, J. Fan and P. Zhao, *J. Mater. Sci.: Mater.*, **29**, 8729 (2018).
39. M. F. Atitar, A. Bouziani, R. Dillert, M. El Azzouzi and D. W. Bahnemann, *Catal. Sci. Technol.*, **8**, 985 (2018).
40. M. A. Messih, M. A. Ahmed, A. Soltan and S. S. Anis, *J PHYS CHEM SOLIDS.*, **135**, 109086 (2019).
41. V. R. Đokić, J. Vujovic, A. D. Marinković, R. Petrovic, D. T. Janaćković, A. E. Onjia and D. Ž. Mijin, *J. Serb. Chem. Soc.*, **77**, 1747 (2012).
42. S. A. Ansari, M. M. Khan, M. O. Ansari, J. Lee and M. H. Cho, *J. Phys. Chem. C.*, **117**, 27023 (2013).
43. R. Chauhan, A. Kumar and R. P. Chaudhary, *J. Solgel Sci. Technol.*, **63**, 546 (2012).
44. T. J. Whang, M. T. Hsieh and H. H. Chen, *Appl. Surf. Sci.*, **258**, 2796 (2012).
45. I. Udom, Y. Zhang, M. K. Ram, E. K. Stefanakos, A. F. Hepp, R. Elzein and D. Y. Goswami, *Thin Solid Films*, **564**, 258 (2014).
46. S. A. Ansari, M. M. Khan, J. Lee and M. H. Cho, *J. Ind. Eng. Chem.*, **20**, 1602 (2014).
47. M. N. Cardoza-Contreras, A. Vásquez-Gallegos, A. Vidal-Limon, J. M. Romo-Herrera, S. Águila and O. E. Contreras, *Catalysts*, **9**, 165 (2019).
48. X. Li, S. He, X. Liu, J. Jin and H. Meng, *CERAM INT.*, **45**, 494 (2019).
49. F. Hosseini, A. Kasaeian, F. Pourfayaz, M. Sheikhpour and D. Wen, *Mat. Sci. Semicon Proc.*, **83**, 175 (2018).